THE ASTROPHYSICAL JOURNAL, 347:656–673, 1989 December 15

IMPLICATIONS OF Ca II EMISSION FOR PHYSICAL CONDITIONS IN THE BROAD-LINE REGION OF ACTIVE GALACTIC NUCLEI

G. J. FERLAND
Department of Astronomy, Ohio State University
AND
S. E. PERSSON
Observatories of the Carnegie Institution of Washington
Received 1988 October 4; accepted 1989 June 20

ABSTRACT

This paper summarizes observations of Ca II emission from active galactic nuclei (AGNs) and discusses their implications for conditions in the emitting gas. Observations of Ca II K and H, the infrared triplet, and the forbidden lines near 7300 Å are compiled to give a "standard" set of line ratios for AGNs with relatively strong Fe II emission. A series of photoionization calculations is presented which examines the conditions needed to produce the observed emission. We pay special attention to the inclusion of heating due to free-free and H^- absorption, processes which couple the near-infrared to millimeter continuum with the emitting gas. These are often the main agents heating the clouds at large column densities. A mean continuum, deduced by Mathews and Ferland and extending from 1 mm to 100 MeV, with a "blue bump" peaking at roughly 60 eV, is used. Regardless of density or ionization parameters, thin clouds (with column densities $\sim 10^{23}$ cm^{-2}) cannot produce the observed Ca II emission. The calculations show that the C III] λ1909/C IV λ1549 intensity ratio *is not* a good indicator of the ionization parameter for this continuum; for large ionization parameters carbon and oxygen Strömgren spheres form, and the C III]/C IV line ratio is double-valued. Clouds with large column densities and ionization parameters, which use an ionizing flux deduced from line reverberation studies, largely reproduce the observed carbon, calcium, and hydrogen spectrum. These calculations suggest a very different picture of BLR clouds than some previous studies. Very large column densities are required to reproduce the Ca II spectrum; indeed, the calculations show that the observed line spectrum imposes no limit on how large this might be, just as the carbon spectrum imposes no limit on the ionization parameter. An important result is that cloud pressure is entirely dominated by radiation pressure. This suggests that the clouds are not stable, while the large column density suggests that the clouds might be a wind or corona above a star or accretion disk.

Subject headings: Ca II emission — galaxies: nuclei — galaxies: Seyfert — quasars

I. INTRODUCTION

The broad-line region (BLR) of Seyfert 1 galaxies and QSOs is thought to consist of a large number of distinct clouds with typical density $\sim 10^{10}$ cm^{-3} and photoionized by a roughly power-law continuum. Observed line ratios constrain the ionization parameter U (the ratio of ionizing photon density to hydrogen number density) to be $\sim 10^{-2}$. Recent work on the interpretation of the spectra of AGNs indicates that this standard picture may not hold up under closer scrutiny. First, rapid time variations in BLR emission lines seem to place the clouds closer to the ionizing source than previously believed (e.g., Peterson 1988), thus requiring much higher density clouds to preserve the ionization parameter at the canonical value. However, such clouds will violate certain density-sensitive line ratios (Rees, Netzer, and Ferland 1989). Second, Mathews and Ferland (1987) have explored some of the consequences of calculating the thermal equilibrium of gas irradiated with a more realistic (softer) ionizing energy distribution than has been assumed heretofore, and this has led to fundamental inconsistencies with the basic idea of pressure confinement of the clouds. Third, there exist two "budgetary" problems with the total amount of line emission: optical Fe II lines in AGNs are often much stronger than can be accounted for by current photoionization models (Netzer 1985; Wills, Netzer, and Wills 1985), and the total line emission relative to Lyα is also higher than can be accounted for by the (supposedly) available energy in the ionizing continuum (Netzer 1985; Collin-Souffrin 1986).

It is the purpose of this paper to present the results of a new series of ionization model calculations for the BLR, carried out to explore these problems more closely. We assume that the basic photoionization picture is correct, but explore that region of parameter space necessary to understand, to first order, the production of emission lines in very low ionization gas, particularly the calcium infrared triplet at 8498, 8542, and 8662 Å. The neutral gas that emits the Ca II lines is strongly shielded from the incident ionizing radiation of the central source—it in fact may be the most strongly shielded material accessible to observation spectroscopically—and is thus a diagnostic that probes very high column density material. As will be made clear, the Ca II infrared triplet offers a simple alternative to Fe II in studying the warm neutral gas in the BLR: the extreme complexity of the energy level structure of the Fe^+ ion and uncertainties in the basic atomic data make theoretical model calculations very difficult, and the emission-line blending makes the extraction of width and strength parameters from spectra uncertain. The Ca^+ ion, by contrast, is far simpler, with only three multiplets arising from five levels plus the continuum to consider, and the atomic data are very well known. The three lines of the infrared triplet are sufficiently separated so that line profile information can be obtained

for FWHM line widths less than ~ 2500 km s^{-1}. The gas that emits the Ca II lines is basically the same as that responsible for Fe II emission but, if anything, it arises from regions that are deeper within the neutral zone (because of the lower ionization potential). A suggested answer to the "Fe II problem" is that a cool, *nonradiatively heated* zone is required (Grandi 1983; Netzer and Wills 1983; Wills, Netzer, and Wills 1985; Netzer 1985; Collin-Souffrin *et al.* 1986; Joly 1986). This solution can be tested by examining the ionization and heating requirements of Ca^+. Because it will be possible to obtain high-quality velocity profiles (in some cases, more easily than characterizing the width of the Fe II lines), the combination of ionization constraints together with the kinematic information may rule out certain geometrical arrangements of BLR gas.

The observational constraints imposed by Ca II emission are combined with previously noted problems with conventional BLR models: (*a*) the C IV λ1549/C III] λ1909 intensity ratio is said to imply an ionization parameter which is inconsistent with continuum flux levels inferred by continuum-line reverberation studies (see, for example, the review by Peterson 1988); (*b*) the low-ionization parameter said to be implied by the carbon line ratios does not reproduce the observed intensities of high ionization lines such as O VI λ1034 (see, for example, the review by Davidson and Netzer 1979); (*c*) the general inability to account for intensities of low ionization lines (which are produced in the neutral zone) relative to Lyα or high ionization lines. This problem is stressed by Collin-Souffrin (1987) and by Wills, Netzer, and Wills (1985); (*d*) the inability to reconcile the total cooling per recombination of the emission-line regions with the inferred ionizing continuum (Netzer 1985).

In this paper, we present photoionization models of the BLR which examine in detail the consequences of (*a*) the mean ionizing continuum deduced by Mathews and Ferland (1987); (*b*) ionization parameters much larger than "standard," but consistent with measurements summarized by Peterson (1988); (*c*) column densities much larger than "standard." We take care to incorporate the heating and ionization effects of both gamma-ray and infrared continua; the latter produces both free-free and H^- heating and is an effective agent in heating neutral gas. Large column densities bring the hydrogen lines into general agreement with the observed Lyα/Hβ ratio (e.g., Baldwin 1977), and largely solve the energy budget problem posed by Netzer (1985; see also Collin-Souffrin 1986; Collin-Souffrin and Lasota 1988). Heating by the gamma-ray and infrared continuum at deep regions of large column density clouds produce strong low ionization lines without the need to invoke nonradiative heating. A large ionization parameter results in the successful prediction of the strength of the high ionization lines.

We begin with a summary of the observational constraints provided by the calcium lines. We then outline our treatment of calcium in the photoionization code, keeping in mind the basic question of what the physical conditions must be in the gas responsible for Ca II triplet emission. Next we extend the model to very high column density; this requires the inclusion of a number of processes which we detail. The primary problem is to heat the gas sufficiently once the ionization has been lowered enough to allow Ca^+ to exist in sufficient quantity not only to provide the line fluxes, but also to insure that the transitions are optically thick. Inclusion of the heating effects of H^- ions and free-free opacity is the key ingredient that leads to a solution that does work. Finally, we discuss the theoretical and observational consequences.

II. THE Ca II SPECTRA OF AGNs

The Ca II triplet lines in AGNs have been largely ignored until recently, mainly because of a lack of suitable (CCD) detectors and spectrographs and the difficulty of working through a maze of atmospheric emission and absorption features. Phillips (1976) first detected the Ca^+ *forbidden* lines at 7291, 7324 Å in the prototype Fe II emitter I Zw 1, Boksenberg *et al.* (1978) were the first to detect the Ca II triplet lines in an AGN (Mkn 231) (this has been confirmed by Hamilton and Keel 1987), and Persson and McGregor (1985) established their presence in I Zw 1. Halpern and Oke (1987) probably detected the lines in Mkn 507 and possibly in 5C3.100, though their spectra do not convincingly show all three lines in either case. Morris and Ward (1988, private communication) detected the triplet lines in Mkn 1365 and IRAS 1249 − 13, and confirmed it in Mkn 1239.

Recently, Persson (1988; hereafter P88) conducted a survey for Ca II emission in 40 AGNs, with the result that the infrared triplet was clearly detected in nine objects and probably detected in five more. There were two selection criteria aside from those imposed purely by the observational considerations of galaxy brightness and redshift. The first was that the emission lines be relatively narrow so that blending with O I λ8446 was not too severe. Second, the objects were selected to have Fe II emission; the high end of the range of Fe II/Hβ was favored. In all of these studies several observational difficulties, plus the possible presence of stellar Ca II absorption, make certain detection of the Ca II triplet lines difficult unless they are strong. It is, therefore, entirely possible that Ca II triplet emission is more prevalent (though weak) than the survey of P88 would indicate. In any case, it is not an *uncommon* phenomenon in Seyfert 1 galaxies and QSOs.

The models were constructed with a "standard" AGN spectrum in mind. We will refer mainly to the list of objects in Table 4 of P88, which comprises the 14 Ca II emitters and the 11 nonemitters with spectra of sufficient quality to establish good upper limits on the strength of Ca II emission. In the following paragraphs, we also add unpublished data on upper limits of several other relevant emission lines. We follow Shine and Linsky's (1974) nomenclature in referring to the triplet lines as X, Y, and Z; Figure 1 shows an energy level diagram. Henceforth XYZ will indicate the sum of the triplet line strengths. A successful ionization model for calcium in AGNs should reproduce the following properties, which are summarized in Table 1. Appendix A and Table 4 contain many of the details concerning the line fluxes and upper limits that went into Table 1.

1. *Line strength.*—The deeply shielded Ca^+ zone must produce enough line emission to yield XYZ/H$\beta \sim 0.2$.

2. *Line optical depth.*—Because the three lines of the triplet are always observed to be equal in strength, the transitions are optically thick. This statement applies, to within the uncertainties, to all the AGNs in which the triplet lines are seen (P88), though it is not necessarily the case in other astrophysical settings (e.g., Herbig and Soderblom 1980). No matter how the Ca II emission zone or zones are distributed, or what the range of physical conditions is represented, only an insignificant fraction of the emission can come from gas that is optically thin in the Ca II lines.

3. Ca II H *and* K *line emission.*— These lines are not seen in AGNs generally, although several systematic effects make detection of these lines difficult. Appendix A and Table 4 collect 11 upper limits and one measurement of the strength of

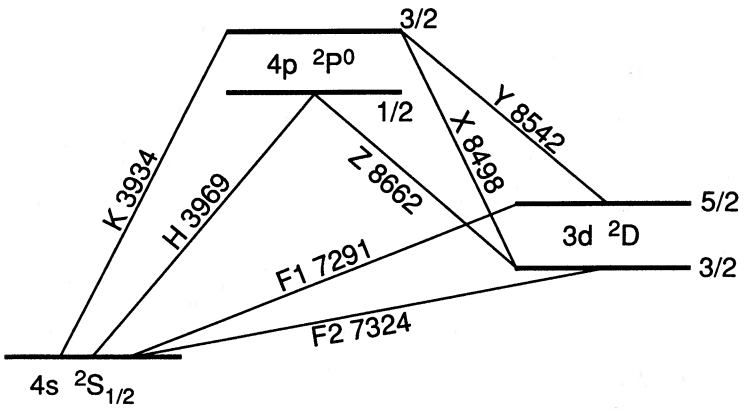

FIG. 1.—Energy level diagram for Ca^+ illustrating lines and nomenclature. Radiative and collisional processes between all five levels and the continuum, including both continuum and (where applicable) line photoionization, are included in the calculation of ionization and thermal equilibria.

the K line as determined from published spectra. A typical 3 σ upper limit has the Ca K/XYZ < 0.20. This includes an assumed reddening to the BLR of 0.25 in E_{B-V}, following the results of De Zotti and Gaskell (1985). If the reddenings are actually smaller, the upper limits to Ca K/XYZ are smaller yet. This constraint is important because it is insensitive to the (unknown) abundance of calcium in the BLR. Henceforth, KH will indicate the sum of the K and H line strengths.

4. [Ca II] *lines.*—The forbidden Ca II lines at 7291, 7324 Å (henceforth F1 and F2; see Fig. 1) are not seen; typically F1 + F2/XYZ < 0.15. See Appendix A for details.

5. Ca II/O I *ratio.*—There is a large range in the ratio of XYZ to the Lyβ–pumped λ8446 line of O I. The median value for the Ca II emitters has XYZ ~ the O I line strength. The correlation of the line widths of Ca II and O I (Fig. 8 of P88) shows that the Ca II and O I emission arise in roughly the same region of the BLR, but because O I is pumped by Lyβ, they do not come from *precisely* the same gas.

6. Ca II/Fe II *ratio.*—If the Ca II triplet is detected, XYZ correlates approximately with the strength of Fe II emission, as measured from the λ5190 and 5320 blends. Figure 7 of P88 shows the dependence graphically.

7. *The X-ray continuum.*—X-ray data were compiled from the literature to check for a difference in optical-to-X-ray continuum slope α_{ox} between the Ca II emitters and nonemitters. Table 1 summarizes the results for X-ray observed objects in

TABLE 1

OBSERVED PROPERTIES OF AGN Ca II EMITTERS

PARAMETER	Ca II EMITTERS			NONEMITTERS
	Minimum	Median	Maximum	Median
XYZ/Hα[a]	0.013 ± 0.006	0.042 ± 0.019	0.11 ± 0.02	<0.01
XYZ/Hβ[a]	0.04 ± 0.02	0.13 ± 0.06	0.34 ± 0.05	<0.03
XYZ/O I[b]	0.35 ± 0.19	1.3 ± 0.3	3.24 ± 0.39	<0.33
XYZ/Fe II[c]	0.05 ± 0.03	0.17 ± 0.11	0.38 ± 0.21	<0.09
KH/XYZ[d]	<0.10	<0.51	<2.8	...
KH/XYZ[d]	<0.05	<0.25	<1.6	...
F1 + F2/XYZ[e]	<0.04	<0.14	<0.18	...
8727/XYZ[f]	<0.01	<0.05	<0.22	...
Fe II/Hβ	0.27 ± 0.04	0.8 ± 0.1	2.5 ± 0.3	0.35
α_{ox}[g]	1.14	1.48	1.71	1.32

[a] XYZ indicates the sum of the strengths of the three lines of the infrared triplet. Values are from Table 4 of Persson 1988, except that in all cases the line ratios have been dereddened by amounts corresponding to E_{B-V} = 0.25, on the basis of the results of De Zotti and Gaskell 1985. For reddening due to the galaxy only, the XYZ/Hβ ratios increase from the tabulated values by a factor of ~1.5 in most cases.

[b] O I is the strength of the O I λ8446 line.

[c] Fe II is the sum of the strengths of the blends around 5190 and 5320 Å. The same comments about the reddening apply.

[d] KH indicates the sum of the strengths of Ca K and H; the limits are 3 σ. Only K can be detected because the H line is confused with Hϵ and [Ne III]. Table 4 contains the 3 σ upper limits from the literature; it has been measured only in I Zw 1 with any certainty (Phillips 1976). The first row corrects for a reddening of E_{B-V} = 0.25, the second only for galactic reddening; see Table 4.

[e] F1 + F2 is the sum of the strengths of the forbidden Ca lines at 7291, 7324 Å. See text and Table 4 for details.

[f] The [C I] λ8727 line upper limits are in Table 4.

[g] α_{ox} is the optical-to-X-ray spectral slope. Values of the soft X-ray fluxes are from the compilation of Dahari and De Robertis 1988 and the optical flux densities are from de Bruyn and Sargent 1978. The median β_{ox} values (same as α_{ox}) computed by Kriss, Canizares, and Ricker 1980 for some of the objects agree well with the tabulated values.

the list of 25 galaxies in Table 4 of P88 (14 Ca II emitters and 11 nonemitters). There is no significant difference in the mean or median spectral index, although the nonemitters have a slightly harder spectrum, on average. Thus, to first order, the distinction between Ca II emitters and nonemitters must be due to properties other than the shape of incident *ionizing* spectrum. Likely differences are in properties of the gas, or as we shall show below, the continuum longward of 912 Å.

III. "STANDARD" MODELS

Before discussing specific model calculations, we outline the strategy, or philosophy, behind this work. It is not yet known what physics controls the formation of the broad emission lines of active nuclei (see Netzer 1988). What is the geometry, composition, and energy source of the emitting gas? This problem is one at the forefront of research in nebular physics, and, as discussed below, many processes otherwise encountered only in stellar atmospheres must be included if the numerical simulation is to be complete. Our purpose in doing these calculations is to see whether photoionization equilibrium can, even roughly, reproduce the observed spectrum. As a "target," we take the mean spectrum deduced by Netzer (1985); given the observed spread in line intensities, we consider a factor of 2 mismatch acceptable. We consider only constant density models, with an eye toward simplicity; as we shall see below, we conclude that the geometry is likely to be a wind or corona, and hence unlikely to be characterized by a constant density. Only when it is known that simple models can come close to reproducing the observed spectrum is it warranted to go on to fully self-consistent calculations, such as the flow behind a mass-losing star. For the same reason, we do not consider heavy-element abundances different from the standard mixture described below. It is in this spirit that we proceed.

As a point of reference, BLR models were first computed using "standard" assumptions concerning composition, column density, and geometry. The calculations were performed with the photoionization code described by Ferland and Rees (1988) and Ferland (1988). The "standard" model of BLR clouds is basically that outlined by Davidson and Netzer (1979). The clouds are thought to be small relative to the distance to the central object; perhaps they are a wind or "comet tail" behind a star (Edwards 1980; Penston 1988) or magnetically confined filaments (Rees 1987). They are assumed to be plane-parallel and characterized by (constant) densities in the neighborhood of 10^9–10^{10} cm^{-3}, and column densities $\sim 10^{23}$ cm^{-2}. We will come back to this last assumption below.

a) Calcium

Calcium has been added to the radiative equilibrium code CLOUDY, most recently described by Ferland and Rees (1988) and Ferland (1988). Calcium is assumed to have a relative abundance by number of Ca/H = 2.3×10^{-6} (Cameron 1982). The other abundances used here are 10^5 (He: C: N: O: Ne: Mg: Al: Si: S: A: Fe:)/H = (10^4: 47: 9.8: 83: 10: 4.2: 0.27: 4.3: 1.7: 0.38: 3.3), and are basically solar values. We know of no direct evidence of the actual calcium abundance of the BLR of AGNs, and it would be surprising if it happened to be very close to our adopted value. Because of this uncertainty, we give the greatest weight to reproducing the observed relative intensities of the Ca II lines and relatively less weight to reproducing the intensities of the calcium lines relative to hydrogen or other metal lines. The intensities of individual members K, H and F1, F2 of the respective multiplets are not well known, although it is known that the three members of the infrared triplet usually have nearly equal intensity. Because of this, we first focus attention on relative intensities of entire multiplets rather than individual members.

i) *Ionization Balance*

Photoionization cross sections are from Reilman and Manson (1979) and Shine and Linsky (1974). Rates for both radiative recombination and dielectronic recombination through highly excited Rydberg states are taken from Aldrovandi and Pequignot (1974), Shull and Van Steenberg (1982), and Arnaud and Rothenflug (1985). Collisional ionization rate coefficients are taken from Arnaud and Rothenflug. To the best of our knowledge, rate coefficients for charge transfer or dielectronic recombination through low-lying autoionizing states have not been computed. Charge transfer rate coefficients were computed using the Landau-Zenner approximation and the semiempirical avoided crossing-potential curves of Butler and Dalgarno (1980). These will be the subject of a future paper but have little effect on the calculations presented here. Other ionization mechanisms include inner shell (K and L) photoionization followed by Auger decay (with the appropriate fluorescence yield), collisional ionization by thermal and suprathermal electrons, and recoil ionization of bound electrons by relatively hard X-rays.

ii) *The* Ca II *Model Atom*

The Ca II ion is treated as a five-level atom plus continuum. The model atom is shown in Figure 1 and is similar to that described by Shine and Linsky (1974). Collision strengths for j-mixing collisions are from Saraph (1970). Collision and radiative data for the $4s$–$4p$ transition are taken from the compendium of Mendoza (1983), and all other collision data are from Chidichino (1981) and Saraph (1970). Radiative data for the $3d$–$4p$ and $4s$–$3d$ transitions are from Black, Weisheit, and Laviana (1972); these are in good agreement with the calculations of Osterbrock (1951). The compendium by Shine and Linsky (1974) provides photoionization cross sections for excited levels. Recombination contributions to the population of individual levels are included by dividing the excited state recombination coefficient among the excited levels we consider, according to their statistical weight, and the rules of LS coupling.

Observations of the K, H to X, Y, Z intensity ratios suggest that all Ca II transitions (including the forbidden lines) can become quite optically thick. Radiative transfer is treated with the escape probability formalism, assuming incomplete redistribution.

iii) *Simple Considerations*

The observations show that the infrared triplet X, Y, Z, (RMT 2, 3 ^{2}D–4 $^2P^o$), is strong relative to both the forbidden multiplet F1 (4 ^2S–3 ^2D) and the K and H lines (RMT 1, 4 ^2S–4 $^2P^o$). This observation sets important limits to the density and optical depth of the line-forming region. A simple three-level atom, assuming that the j-levels within the three terms are populated according to their statistical weights, was used to predict the intensities of the three multiplets for a wide variety of temperature and density, but assuming that the lines are optically thin. The atomic data are summarized in the next section, but are largely those given by Shine and Linsky (1974) with a few recent additions. The results of this calculation are

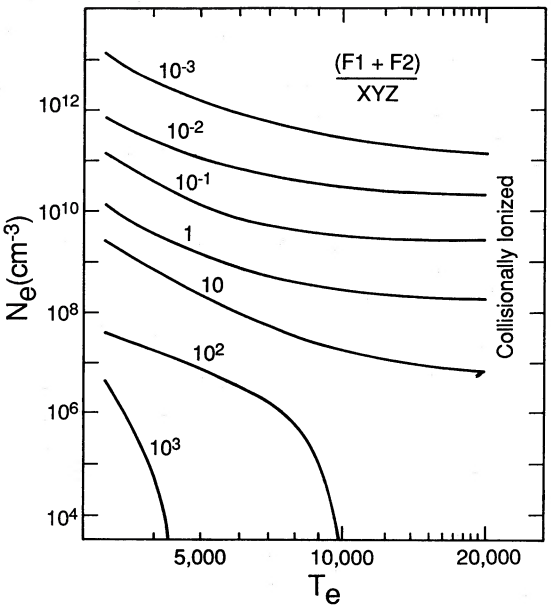

FIG. 2.—Results of a simple three-level atom calculation, showing temperature and density range where Ca II lines are likely to be formed. Line transfer effects are not included, and levels within the three terms are assumed to be well mixed. This calculation shows that densities thought to be typical of the BLR can reproduce the ratio of forbidden to infrared triplet emission.

shown in Figure 2. The temperature range was chosen from simple physical principles; optical emission is not produced for temperatures lower than ~ 3000 K, and Ca^+ is collisionally ionized to Ca^{++} when $T_e \geq 2 \times 10^4$ K (Jordan 1969). The density range goes from densities where the model atom has low density limit populations to well above broad-line region densities. The calculation includes only collisional and optically thin spontaneous radiative decays and does not include much of the physics described below.

Two conclusions, both straightforward, can be reached from these calculations. The first is that line transfer strongly affects the Ca II spectrum. In the optically thin limit, the ratio of KH to XYZ is proportional to the branching ratio out of $4\ ^2P^o$ and is ~ 38, independent of physical conditions. The observations show that this ratio is actually much smaller. The difference could be due to reddening, but the color excess implied ($E[B-V] \sim 2$ mag) is lage and this interpretation will not be pursued further here. Line transfer is the alternative. Transfer affects line ratios when the collisional de-excitation rate $N_e C_{ul}$ is of order the effective lifetime of the upper level, $\sim A_{ul}/\tau_{ul}$. (This assumes that the number of scatterings N_{scat} is $\sim \tau^{-1}$.) For typical BLR densities ($N_e \sim 10^{9.5}$ cm^{-3}), this occurs when $\tau_{KH} \sim 10^{4.5}$. The K, H to X, Y, Z intensity ratio is consistent with simple predictions and BLR expectations if the Ca II lines are quite optically thick.

The ratio of the infrared triplet to the forbidden lines, shown in Figure 2, suggests that the line-forming region has a density in excess of $\sim 10^9$ cm^{-3}. This is required if the forbidden lines are to be weak relative to the infrared triplet. The critical density of $3d\ ^2D$, where the collisional de-excitation rate equals the radiative de-excitation rate, is $\sim 7 \times 10^6$ cm^{-3}. Above this density, the ratio of the infrared triplet to the forbidden lines increases, since F1,2 are collisionally deactivated. The likely detection of the [Ca II] lines in at least one object (see above) suggests that the density is not significantly above 10^{10} cm^{-3}.

These considerations suggest that the Ca II spectrum arises in clouds which are quite optically thick in resonance lines, and which have densities of order 10^9–10^{10} cm^{-3}. These conditions are strongly suggestive of BLR conditions (Davidson and Netzer 1979). The calculations presented in the next sections pursue this idea further; we attempt to model the Ca II spectrum in the context of fairly standard assumptions concerning the BLR.

iv) *Line-Continuum Overlap*

Some of the clouds we consider below have significant continuous opacities. Important continuous opacities include the Balmer and Paschen continua, H^- and free-free absorption, and the $2\ ^3S$, P levels of neutral helium. The effects of line absorption by these continua are included using the formalism described by Elitzur and Netzer (1985), Netzer, Elitzur, and Ferland (1985), and Rees, Netzer, and Ferland (1989). Line destruction by such continua, along with optical depths, are included for all lines explicitly predicted below. Among the processes included are Lyα, Hα, and Pα photoionization of excited states of hydrogen, calcium, helium, the H^- ion, and free-free absorption. In the models considered below, H^- destruction of Hα can amount to as much as half of the produced line. Line pumping of Ca H by Hϵ is included, although this is not a significant line production mechanism in any of the models considered below. Finally, most intercombination and forbidden lines considered in the large column density models presented below become optically thick (most importantly, [O I] λ6300, C II] λ2336, C III] λ1909, and the [Ca II] lines) and these are again transferred using escape probabilities.

v) Ca^+ *Shielding*

The ionization potential of Ca^+ is 11.871 eV, so we expect Ca^+ ions to exist largely in regions which are well shielded from radiation at wavelengths shortward of Lyα (see also Joly 1988). These regions are likely to be largely neutral and have large optical depths to the Ca II lines. However, we shall also see that Ca II lines have significant contributions from regions where Ca^{++} is the dominant stage of ionization, but the Ca II lines are relatively optically thin. The line formation is a trade-off between large fraction abundance and small optical depths, both of which make line formation efficient.

The calculations presented here include the valence and inner shell opacities of all 13 elements included in the calculation, along with absorption due to excited states of several ions. Atomic carbon is the most important opacity source for the calcium ionization balance. Other important opacity sources, which still provide a significant fraction of the shielding of the Ca^+ zone, are electron scattering and the damping wings of Lyα and higher Lyman lines (in the Rayleigh scattering limit). These are scattering opacity sources, and attenuate the incident radiation field as $\sim \tau^{-1}$ rather than as $\sim \exp(-\tau)$.

b) The Incident Continuum

The ionizing continuum we use here is largely that given by Mathews and Ferland (1987), which uses the mean observed optical, ultraviolet, and X-ray continuum, and an inferred "blue bump" peaking at roughly 60 eV (Malkan and Sargent 1982). A major concern is the assumption that the BLR clouds "see" the same continuum we do; it is easy to imagine circumstances where the continuum may be "beamed," or where parts of the infrared continuum arise from dust emission far

outside the BLR. We use the observed continuum despite these reservations. An exception is our choice of the far-infrared and submillimeter continuum, which strongly affects the cloud thermal balance via free-free heating. We discuss this next.

i) H^+ *Free-Free Heating and Cooling*

The treatment of free-free heating in the present calculations is described by Rees, Netzer, and Ferland (1989). The infrared continuum is divided into 200 energy cells, with logarithmically increasing width, which cover the energy interval between a low energy of 1 mm (9.12×10^{-5} Ry) and the ionization potential of the first excited state of hydrogen (0.25 Ry). The free-free heating rate is evaluated by numerically summing over the depth-dependent continuum, which extends to 100 MeV. Free-free Gaunt factors are largely taken from Hummer (1988), and pair production rates are as in Ferland and Rees. The free-free cooling rate is modified as described by Ferland and Rees (1988), with the critical frequency defined there.

ii) *The Submillimeter Break*

The exact energy of the submillimeter break, where the continuum slope changes from $f_\nu \sim \nu^{-1}$ to one with positive slope (which we take to be $f_\nu \sim \nu^2$) affects our calculations, because of the important role played by free-free heating (see Krolik, McKee, and Tartar 1981; Ferland and Rees 1988; Rees, Netzer, and Ferland 1988). The continuum chosen by Mathews and Ferland (1987) extends to 1 mm without breaking, and this seems appropriate for radio objects. Radio-quiet objects seem to have a break between 100 and 370 μm (Engargiola *et al.* 1988), however, As we shall see below, the uncertainty in the energy of the break, a question which will be observationally answered, affects the photoionization calculations a great deal when the ionization parameter is large.

Two parameters, the hydrogen density N_H and the ionization parameter U (defined here as the dimensionless ratio of the density of hydrogen-ionizing photons ϕ_H/c cm^{-3}, where ϕ_H is the surface flux of photons, to hydrogen densities N_H, $U \equiv \phi_H/(N_{H^c})$, characterize BLR clouds according to the standard model. Before proceeding with a detailed examination of the Ca II spectrum, we examine some consequences of changing the wavelength of the submillimeter break in the infrared continuum. Table 2 gives predictions of some of the stronger lines in clouds with two ionization parameters and four choices of the wavelength of the break. In all cases the density is $N_H = 10^{9.5}$ cm^{-3} and the column density is 10^{23} cm^{-2}.

As the wavelength of the break λ_B increases, the importance of free-free heating also increases. The far-infrared luminosity L_{IR} is deposited over depths of order

$$\delta r_{IR} \sim 10^{13}\left(\frac{N_e}{10^{9.5}\text{ cm}^{-3}}\right)^{-2}\left(\frac{T_e}{10^4\text{ K}}\right)^{3/2}\left(\frac{\lambda_B}{100\ \mu\text{m}}\right)^{-2}\text{ cm}\,, \quad (1)$$

for a fully ionized gas. For comparison, the depth over which the ultraviolet luminosity L_{UV} is deposited, which is primarily through photoionization and hence proportional to the classical Strömgren thickness of the cloud, is

$$\delta r_{UV} \sim \frac{Uc}{N\alpha}\,, \quad (2)$$

so the comparative heating rates per unit volume are $(L_{IR}/\delta r_{IR})/(L_{UV}/\delta_{UV}) \sim UN \sim \phi_H$. Free-free heating is relatively more important for higher fluxes or ionization parameters; then the gas is more highly ionized and photoelectric heating (which is proportional to the neutral density) is smaller. In contrast, free-free heating is basically proportional to N_e^2 and does not decrease when the level of ionization increases.

The strongest effect is upon the higher ionization lines which are formed nearer the illuminated face of the cloud. Lines formed in neutral regions are less affected because the far-infrared continuum is attenuated at large column density, and the gas is less ionized there. It is clear from Table 2 that if BLR clouds "see" the same continuum we observe, then differences in the 100 μm–1 mm continuum of radio-loud and radio-quiet objects will also affect the emission-line spectrum at the $\sim$0.5 dex level. Such differences are in fact observed (Grandi and Osterbrock 1977), although it is also known that the ionizing continua differ.

For the present calculations, we use a continuum which has a break at 100 μm. The question of the position of the submillimeter break in radio-quiet versus loud objects is best addressed by direct observation, which should be forthcoming.

c) The Density

Figure 3 shows the results of calculations in which N_H was varied. The calculations are the result of at least three iterations on the ionization structure to ensure that the line optical depths, which are included for all lines predicted, are well defined. Clouds are assumed to have an ionization parameter of $U = 10^{-2}$ and a column density of 10^{23} cm^{-3}. These are close to the "standard" values and were chosen to reproduce the observed C III] λ1909/C IV λ1549 intensity ratio at a density of $10^{9.5}$ cm^{-3} (Davidson and Netzer 1979).

TABLE 2

THE SUBMILLIMETER BREAK

	λ_B							
	10 μm[a]		100 μm[b]		316 μm[c]		1 mm[d]	
LINE	$U = 10^{-2}$	$U = 10^{-1}$	$U = 10^{-2}$	$U = 10^{-1}$	$U = 10^{-2}$	$U = 10^{-1}$	$U = 10^{-2}$	$U = 10^{-1}$
Lyα	100	100	100	100	100	100	100	100
C IV λ1549	39	77	39	82	41	105	48	131
C III λ1909	17	13	17	15	18	18	20	20
N V λ1240	0.2	2.6	0.2	2.7	0.2	3.8	0.3	6.8
O VI λ1034	0.02	3.8	0.02	4.0	0.03	6.2	0.03	14
Mg II λ2798	6.3	1.6	6.4	1.8	6.7	2.1	7.5	2.2

[a] $T_C = 1.26 \times 10^7$ K.
[b] $T_C = 1.05 \times 10^7$ K.
[c] $T_C = 0.97 \times 10^7$ K.
[d] $T_C = 0.92 \times 10^7$ K.

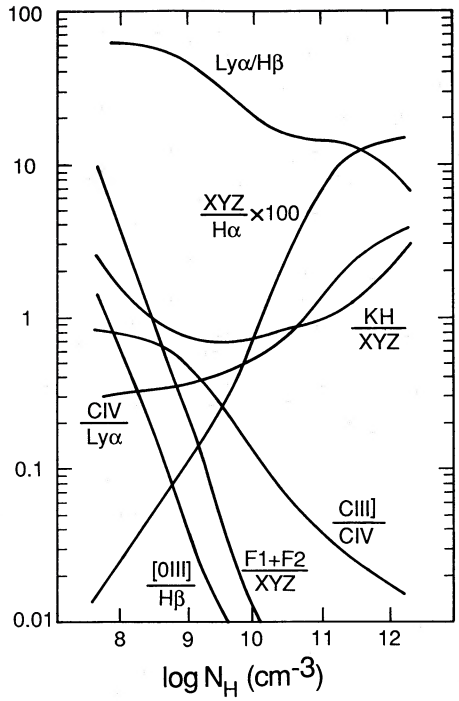

FIG. 3.—Dependence of emergent line ratios as a function of hydrogen density at fixed ionization parameter $U = 10^{-2}$. Column density is held fixed at 10^{23} cm^{-2}. Note that the F1 + F2/XYZ ratio is consistent with observed upper limits only for densities greater than 10^9 cm^{-3} for this column density, and KH/XYZ is predicted to be stronger than observed upper limits at all densities, while the strength of the infrared triplet relative to the hydrogen lines requires $N > 10^{11}$ cm^{-3}.

The C III] λ1909/C IV λ1549 ratio is typically in the ratio 1:3 and is shown in the figure. This ratio is an indication of the level of ionization at low densities and ionization parameters (Davidson 1977), although it is also sensitive to density for N_H greater than $\sim 10^9$ cm^{-3}. This line ratio suggests $N_H \sim 10^{9.5}$ cm^{-3}, although it is important to remember that this prediction is redundant; the density was chosen to reproduce the carbon ratio at the deduced ionization parameter.

Two other line ratios are consistent with densities of order $10^{9.5}$ cm^{-3}. The figure shows the ratio of [O III] λ4363 to Hβ (marked as [O III]/Hβ). The absence of broad λ4363 emission suggests $N_H > 10^9$ cm^{-3} (for example, Davidson and Netzer 1979). The ratio of C IV λ1549 to Lyα is typically ~0.5 and is an increasing function of density because of increased free-free heating and decreased efficiency of Lyα emission (Rees, Netzer, and Ferland 1989). Observed values suggest $N_H < 10^{10}$ cm^{-3}.

The limit to the intensity of the forbidden calcium lines, which are usually not detected, relative to the infrared triplet, is typically I(Ca II F1, F2)/I(Ca II X, Y, Z) ~ 0.2. The figure shows that this suggests a density of $N_H > 10^9$ cm^{-3}, a limit very close to the standard value.

Although the F1, F2 to X, Y, Z ratio does not challenge the standard model in any way, this is not true of the HK lines, or XYZ, relative to Balmer lines. The figure shows the ratio of the infrared triplet to Hα. The mean spectrum considered above gives this ratio as ~0.04, suggesting a density $\sim 10^{10.5}$ cm^{-3}, well in excess of the standard values. Ca II K and H are observed to be weaker than the triplet. As Figure 3 shows, at no density are the model calculations in the neighborhood of the observed values.

The figure shows predicted values of the hydrogen Lyα/Hβ ratio, which is observed to be ~10. As is well known (Netzer 1985) the observed Lyα/Hβ ratio cannot be reproduced by conventional calculations which use the observed continuum, for standard densities. This problem has been known for some time, and could be resolved by either using a continuum harder than that observed (Kwan and Krolik 1981), postulating external reddening (Netzer 1985), or using a high density ($\sim 10^{12}$ cm^{-3}; Hubbard and Puetter 1985). Here again the predictions are in dramatic disagreement with observations.

This section has shown that the relative intensities of lines produced in the ionized zone of the cloud, Lyα, C III] λ1909, C IV λ1549, and [O III] λ4363, suggest densities in dramatic disagreement with those suggested by line arising in the neutral zone; e.g., Ca II and the Balmer lines, for the assumed column density.

d) The Ionization Parameter

Figure 4 shows the results of a series of calculations in which the ionization parameter was varied but the density was held constant at $N_H = 10^{9.5}$ cm^{-3}. The models have a constant Lyman continuum optical depth of 10^5, according to a column density of 1.9×10^{22} cm^{-2} at an ionization parameter of 10^{-2}, and a column density of $\sim 1 \times 10^{23}$ cm^{-2} at an ionization parameter of 10^0. The actual column density of the various models varies because of the changing ionization parameter. The "standard" value of U is in the neighborhood of 10^{-2}, although continuum-line reverberation studies suggest much higher values can occur, as high as $U \sim 10^{-0.5}$ (see, for example, the review by Peterson 1988).

The Lyα/Hβ ratio decreases with increasing ionization parameter since line transfer effects grow more important as the Lyα photon density increases at high flux levels. For the same reason, the radiation pressure, which is computed as in Elitzur and Ferland (1986), increases and exceeds the gas pressure when $U \geq 10^{-1.5}$. BLR pressure at high ionization parameters is completely dominated by radiation pressure. Such a cloud would not be stable it is were supported by an external medium (Ferland and Elitzur 1984), but his scenario is ruled out on other grounds (Mathews and Ferland 1987). The O VI λ1034 line increases in strength as the level of ionization increases with increasing ionization parameter (Baldwin and Netzer 1978; Davidson and Netzer 1979).

Once again, the predicted Ca II spectrum is in serious disagreement with the observations; only at the highest ionization parameters does the ratio of K, H to X, Y, Z fall below unity. At no value is the XYZ/Hβ ratio within an order of magnitude of the observed value.

The most surprising result of these calculations is the behavior of C III] λ1909/C IV λ1549. Previous studies found that this line ratio was a monotonically decreasing function of U for low values of the parameter. Our calculations reproduce this behavior up to an ionization parameter of $U \sim 0.1$, but for larger values of U the ratio actually increases. This is largely due to the formation of a highly stratified set of carbon and oxygen Strömgren spheres, along with the effects of excited state photoionization of helium.

Figure 5 shows the ionization structures of two clouds, the upper having the conventional ionization parameter ($U = 10^{-2}$), and the lower having the higher ionization parameter suggested by some reverberation studies ($U = 10^{-0.5}$). As is well known, C^{+2} and C^{+3} largely coexist at low ionization parameters (Davidson and Netzer 1979). Increasing U under

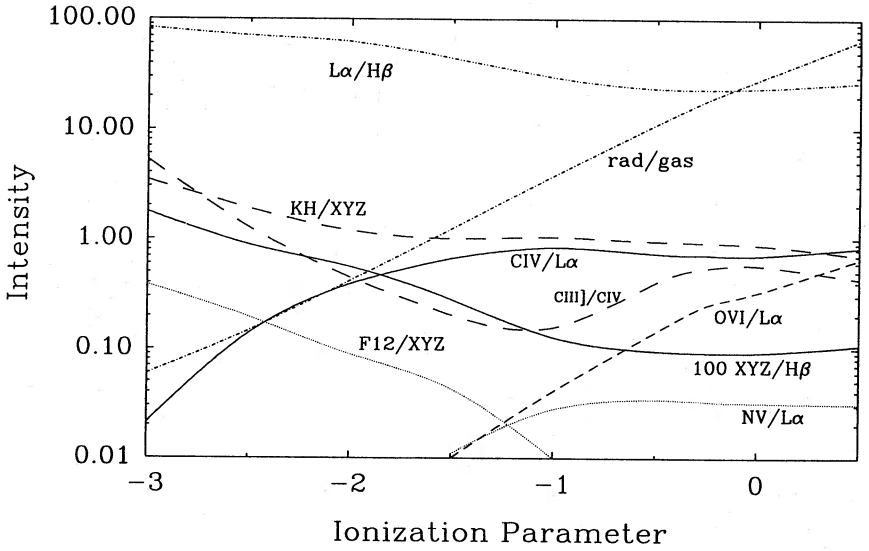

FIG. 4.—Dependence of emergent line ratios as a function of ionization parameter for a fixed hydrogen density $N_H = 10^{9.5}$ cm^{-3}. Optical depth in the Lyman continuum was held fixed at 10^5, corresponding to column densities of roughly 10^{22} cm^{-2} and 10^{23} cm^{-2} at ionization parameters of 10^{-2} and 10^0. Again, no value of the ionization parameter can reproduce the full Ca II spectrum.

these conditions increases the level of ionization, and hence decreases the C III] λ1909/C IV λ1549 intensity ratio. This trend continues until carbon-oxygen Strömgren spheres form, and carbon-oxygen self-shielding becomes important (lower panel, Fig. 5).

Simple considerations (Osterbrock 1974) suggest that increasing the ionization parameter increases the scale of the entire ionization structure linearly (i.e., the Strömgren length is proportional to the number of ionizing photons, other things being equal). This length is given by

$$\delta r = \frac{\phi}{N^2 \alpha} = U \frac{c}{\alpha}, \tag{3}$$

where α is the recombination coefficient and ϕ is the flux of ionizing photons. The high ionization parameter model on the bottom of the figure has a radial scale which has been shifted by 1.5 dex, the ratio of the ionizing parameters, to compare more easily the two calculations. Because of the renormalization, if nothing else varied the two ionization structures would be identical.

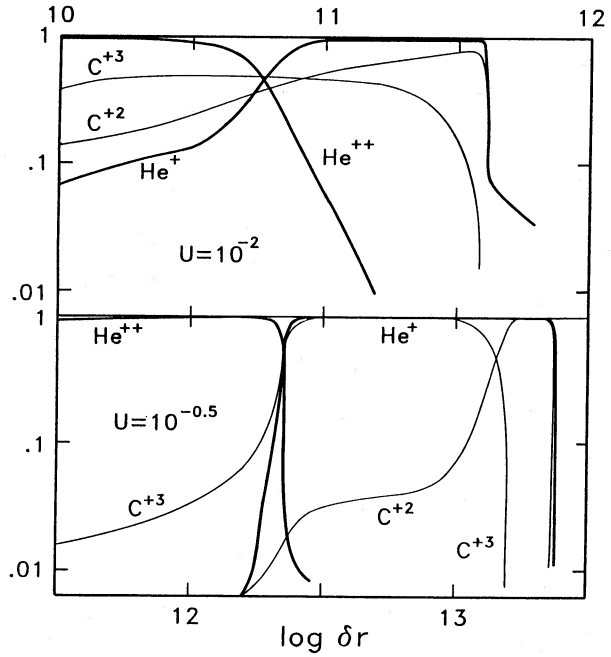

FIG. 5.—Ionization structures of clouds with two values of the ionization parameter. Radial scale has been shifted by the ratio of the ionization parameters to more easily compare the two structures. An extended ionized helium zone, in which carbon is mainly in the form C^{+2}, occurs for high ionization parameters because of absorption of the ~50 eV continuum by C^{+3} and photoionization of the $2\,^3S$ state of helium by both the incident continuum and optically thick lines, especially Lyα. As a result, the C III] λ1909 line remains strong even at the high ionization parameters suggested by line-continuum reverberation studies.

The figure shows both the helium and carbon ionization structures. As expected, the He^{+2}–He^+ ionization fronts occur at nearly the same scaled radius, and the front is less well defined at the lower ionization parameter. This is because the thickness of an ionization front is typically of order a mean free path of an ionizing photon, $t \sim (N_0 \sigma)^{-1}$, where N_0 is the neutral species and σ is the photoionization cross section. The relative thickness of the ionization front, $t/\delta r$, then decreases as U^{-1} (Davidson and Netzer 1979), and high ionization parameter clouds tend to have sharp fronts.

The He^+–He^0 ionization fronts do not occur at exactly the same scaled thickness, however, because of the increased radiation density. The strongest effect on the ionization structure is caused by photoionization of He^0 $2\,^3S$ and $2\,^3P$ by both the incident continuum and trapped lines such as Lyα. At the higher ionization parameter, the majority of the triplet recombinations do not eventually populate the singlets, but rather are photoionized before exchange collisions or radiative decay occurs. Other effects which enter at high ionization parameters are stimulated emission and induced recombination. For instance, the stimulated emission correction to the optical depths in the Balmer continuum or $2\,^3S$ amount to ~20%, and are even larger for more highly excited states.

Carbon and oxygen Strömgren spheres form at large ionization parameters. For high ionization parameters, carbon is almost entirely in the form of C^{+3}, and oxygen O^{+2}, near the

illuminated face of the He^+ zone. It is easy to show that these ions of C and O compete very effectively with helium in absorbing the continuum between 24.6 and 54.4 eV, and that the typical mean free path of C or O ionizing photons is $\sim 10^{12}$ cm. As a result, well-defined ionization fronts occur when the ionization parameter (and hence Strömgren thickness) is large. Once such a well-defined set of ionization zones occurs, the relative abundances of C^{+3} and C^{+2} no longer depend on the ionization parameter, for much the same reason that the He I/He II spectrum depends mainly on the shape of the ionizing continuum (Osterbrock 1974). The change in the carbon 1909/1549 line ratio at large U is largely due to radiative transfer effects; the Balmer and He triplet continuous opacity is significant and absorbs the lines to some extent. Further, the optical depths in both the λ1909 and λ1549 lines becomes large enough to affect the line strengths. The full range of predicted carbon line ratios is similar to the observed range in high-redshift objects (Baldwin, Wampler, and Gaskell 1989) when $U > 0.1$. This has the important implication that BLR clouds need not have their parameters "fine tuned" to reproduce the observed spectrum.

e) *Initial Conclusions*

The discussion above contains mixed results. A surprising prediction is that, given our composition and ionizing continuum, a wide range of ionization parameters is actually allowed by the observed C III] λ1909/C IV λ1549 intensity ratio. This solves a long-standing problem; it is no longer necessary to postulate a "hidden hand," which "fine-tunes" the ionization parameter to a special value. Large values, which are suggested by both line-continuum reverberation studies and the observed O VI λ1034 intensity, are also consistent with the carbon spectrum.

These calculations did not come close to reproducing the Ca II emission, however. Hydrogen and iron line spectra have long suggested that something is wrong with our assumptions concerning the BLR, but a completely reliable calculation of the emergent H I or Fe II spectrum of a realistic cloud is not yet in hand (Avrett and Loesser 1988; Collin-Souffrin 1987; Hubbard and Puetter 1985; Netzer 1985; Wills, Netzer, and Wills 1985). A realistic calculation of the hydrogen spectrum must include the full transfer of all $\sim$400 optically thick lines included in the present calculation. This has yet to be done, but is trivial compared to a comparable calculation of the Fe II spectrum, where tens of thousands of transitions between hundreds of levels must be considered (Wills, Netzer, and Wills 1985).

In contrast, the Ca II spectrum points out a major problem with BLR calculations in a very simple way. The ultraviolet Ca II lines are predicted to be far too strong relative to the infrared lines. One possibility in explaining the hydrogen and iron spectra, in which the ultraviolet Lyα is also observed to be much stronger than expected relative to other lines, is that our line of sight to the BLR is moderately reddened by dust outside the BLR (for example, Netzer 1985). The conflict between observed and predicted Ca II K, H/X, Y, Z ratios requires a reddening of $E(B - V) \sim 2$ mag, far larger than that suggested by the hydrogen spectrum.

The hydrogen spectrum can be reproduced if we postulate that the ionizing continuum striking the BLR is actually much harder than observed from Earth (Kwan and Krolik 1981). Tests show that even radical changes in the ionizing continuum; i.e., even as extreme as that chosen by Kwan and Krolik, alter the predicted K, H/X, Y, Z ratio by less than a factor of 2. Again, the solution to the Ca II problem must lie elsewhere.

An obvious possibility is the possibility that dust is mixed with the BLR gas. In this case, multiple scatterings could destroy K, H (because of the larger line optical depth, and larger dust cross section at $\sim$3900 Å) and not affect the intensity of the infrared triplet a great deal. The possibility of dust mixed with the emitting gas was discussed in detail some time ago as a way to explain the low value of Lyα/Hβ (for instance, Shuder and MacAlpine 1979; Ferland and Netzer 1979). This, however, will not solve the problem of the intensities of XYZ relative to the Balmer lines since Lyα is weakened relative to weak intercombination lines (Ferland and Netzer 1979). This latter problem is more than an order of magnitude. We must look elsewhere to account for the XYZ/Hβ ratio.

IV. LARGE COLUMN DENSITY CLOUDS: ASSUMPTIONS AND RESULTS

The discussion in the previous section underscores several problems with conventional models of the BLR. For clouds dense enough to produce the observed hydrogen line spectrum, the carbon spectrum is not reproduced. At all densities, the Ca II K and H lines, relative to the infrared triplet, are predicted to be over an order of magnitude stronger than observed. The basic requirement to reproduce the observed Ca II spectrum is to deposit large amounts of heat at very large optical depths. In this case, the optical depth in the K and H lines will be large enough for these lines to be thermalized, while the infrared triplet will continue to be produced.

This requirement is closely related to two problems previously noted; Netzer (1985) found that the "energy budget," or amount of heat deposited in a BLR cloud per hydrogen ionization, was much larger than expected from the observed ionizing continuum, given the assumptions of the standard model. This problem could indicate that the observed spectrum has been reddened by dust outside the emission-line region, or that the column density is much larger than usually assumed. Kwan and Krolik (1981) had previously shown that the observed hydrogen emission-line spectrum could be reproduced at the density suggested by the carbon spectrum, but used a very hard continuum, with a 2 keV/2000 Å flux ratio roughly 10 times larger than the mean (Zamorani *et al.* 1982; Netzer 1985). The problem here too is to reconcile the observed continuum with the observed emission-line spectrum.

We saw above that the Ca II spectrum cannot be reproduced over a wide range of density and ionization parameters, given the assumed column density. This section concerns conditions in clouds with very large column densities. Appendix B describes the changes made to the radiative equilibrium code CLOUDY to treat such very thick clouds.

a) *Heating Processes*

The question of whether radiative heating alone can support the ionization and thermal structure of BLR clouds, or whether nonradiative processes operate, is a fundamental one. Before proceeding, we compare the relative importance of the several processes which heat matter at large column densities. Figure 6 compares several processes for clouds with densities of $10^{9.5}$ cm^{-3}, various ionization parameters, at a Lyman continuum optical depth of 10^7. Heating is expressed as a fraction of the total heating at that point.

Traditional ionizing radiation is nearly fully absorbed at the point in question, and heating is mainly provided by processes

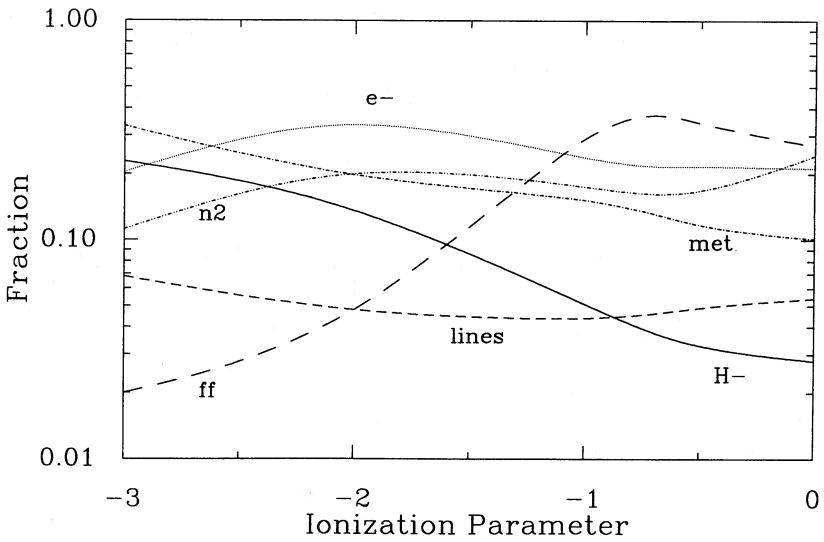

FIG. 6.—Heating sources at large optical depth. Figure shows the relative heating rates for various processes and ionization parameters at a large Lyman continuum optical depth (10^7) into the cloud. Traditional nebular heating sources (ground-state photoionization of hydrogen and helium) are negligible at this depth. The term "lines" indicates the fraction of the heating due to hydrogen line destruction by various continuous opacities, "ff" is the free-free heating (the most important at large ionization parameters), "met" is metal photoionization (mainly the valence shell of C^+ and the K, L shells of Fe^+), "*e*-" is Compton scattering of bound electrons, "n2" is photoionization of excited states of hydrogen (mainly the first excited state), and "H-" is heating due to photodissociation of the negative hydrogen ion.

which couple the infrared and hard X-ray radiation fields to the gas. Compton scattering of bound electrons (the curve marked "*e*-") is among the more important for all ionization parameters (Bethe and Salpeter 1957; Collin-Souffrin, Hameury, and Joly 1988). This occurs mainly as the result of absorption of the ~2–100 keV continuum. The ultraviolet continuum heats the gas mainly by photoionization of the heavy elements (the curve marked "met"). This is mainly absorption of the 11 eV continuum by atomic carbon, and of the X-ray continuum by the K and L shells of iron. Direct photoionization of the hydrogen atom is mainly from the first excited state, and this is an effective heating agent, especially at high ionization parameters (the curve marked "n2"). Free-free heating, mainly by absorption of the ~10–100 μm continuum (the curve marked "ff") is the main heating mechanism at high ionization parameters, while heating due to photodissociation of the negative hydrogen ion by the ~1 μm continuum (the curve marked "H-") is a major heating mechanism at lower ionization parameters (see, for example, Avrett and Losser 1988). Once created, line photons such as Lyα or the Balmer lines undergo multiple scattering before escaping, and these photons can be absorbed and heat the gas as the result of free-free, H^-, and Balmer-Paschen continuous opacity. The curve marked "lines" shows the relative importance of this effect. Many of these processes, especially free-free and H^- heating, are the dominant heating mechanism for some conditions.

b) A Thick Cloud

Figure 7 shows the results of a series of calculations in which the column density of a cloud with a constant hydrogen density of $10^{9.5}$ cm^{-3} is illuminated with the mean AGN continuum discussed above. The column density is increased above the canonical value of 10^{23} cm^{-2}. An ionization parameter of log $(U) = -0.5$ was chosen. This was based on our assumed hydrogen density, and the λ1280 continuum flux at the BLR radius in Akn 120, as measured by Peterson and Gaskell (1989). The figure shows the emergent spectrum from clouds with various values of the column density.

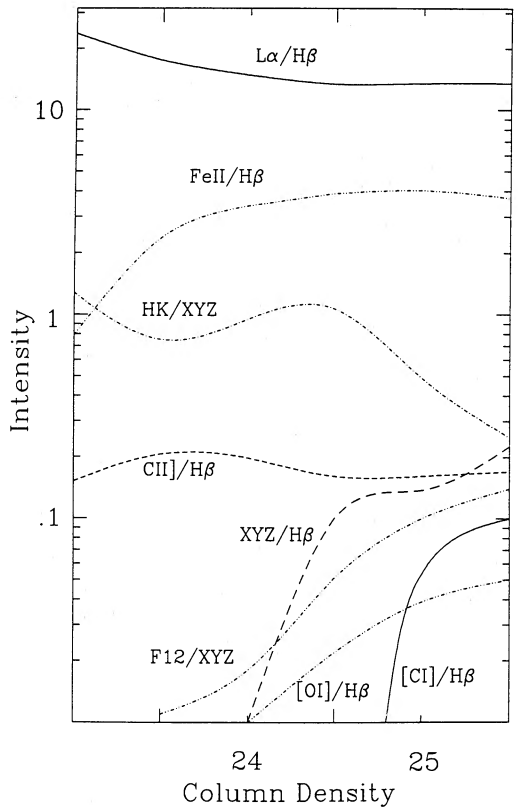

FIG. 7.—Emergent line ratios from a series of model clouds are shown as function of the column density. Ca II emission requires $N_H > 10^{24.5}$ cm^{-2}.

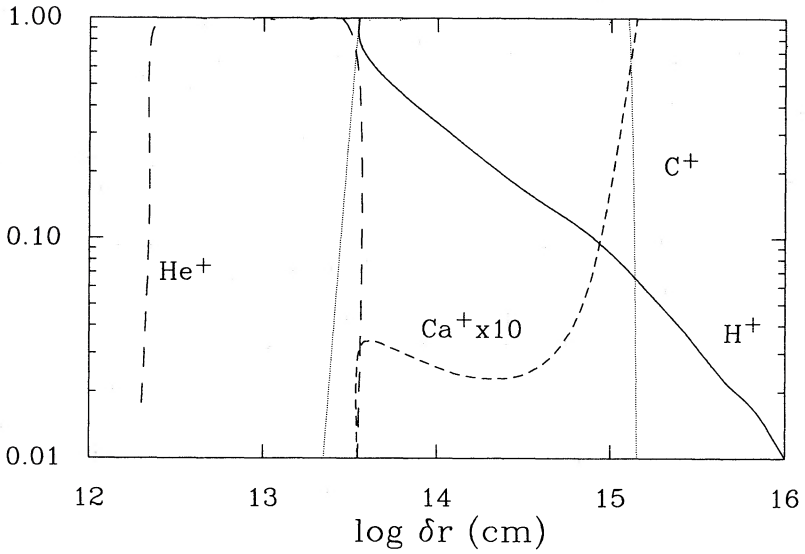

FIG. 8.—Ionization fraction of various species vs. distance into the cloud for a fixed density of $10^{9.5}$ cm^{-3}.

Figure 8 shows the fractional ionization of He^+, H^+, C^+, and Ca^+ (the last multiplied by a factor of 10) in a cloud with a column density of $10^{25.5}$ cm^{-2}. Helium is fully ionized up to a cloud thickness of $\delta r \approx 10^{12.7}$ cm (the distance from the illuminated edge of the cloud is indicated at the bottom). Hydrogen remains fully ionized, and helium singly ionized, until the hydrogen ionization front occurs at depth of $\delta r \approx 10^{13.6}$ cm. Finally, the C^+–C^0 ionization front occurs at a depth of $\delta r \approx 10^{15.2}$ cm). A trace level of ionization of hydrogen persists beyond the H^+–H^0 ionization front because of the combined effects of photo and collisional ionization from excited states of resonance fluorescence in the Lyman lines (which helps populate excited states), and because of secondary ionization by suprathermal electrons. The C^+–C^0 ionization front occurs when the continuum shortward of Lyα has been nearly fully absorbed by the combined opacity due to atoms of C, Mg, Al, Si, S, Fe, atoms and ions of Ca^0 and Ca^{2+}, the damping (Rayleigh scattering) wings of Lyα and higher Lyman lines, and continuous absorption in the Balmer and He I $2\,^3S$ continua.

Calcium is predominantly in the form Ca^{2+} throughout much of the C^+ zone; only when the C^0 ionization front occurs does Ca^+ become the dominant ionization stage. The fractional abundance of Ca^+ depends on the electron density; as the ionized hydrogen decreases and the electron density falls, the recombination rate to form Ca^+ decreases and the ionization increases. Eventually, in deeper regions of the cloud, shielding is sufficient to allow C^0 and Ca^+ to exist. The computed temperature is typically 4000–5000 K at this point.

Figure 7 shows the emergent emission-line spectrum for clouds of various column densities. The effect of increasing the column density is, as expected, to strengthen lines from ions with low ionization potentials. We focus attention on Hβ and Lyα, and the intensities of other lines relative to these. The Lyα/Hβ ratio decreases as the column density increases because the intensity of Hβ increases; Lyα has saturated by the time a column density of 10^{23} cm^{-2} is reached; increasing the column density further increases mainly the Balmer and higher lines. The Lyα/Hβ ratio decreases to $\sim$13 at large column densities; this is nearly in agreement with observed BLR ratios, although it is still a bit high. The Hα/Hβ ratio is weakened by H^-, f-f, and f-b opacity. The total continuous optical depth at the wavelength of Hα is well over unity. Table 3 gives predictions of a model with a column density of $10^{25.5}$ cm^{-2}.

The calcium spectrum provides an important constraint on the column density; it must be large in these Fe II–loud objects. The ratio of the K and H lines to the infrared triplet remains nearly constant until the K and H lines become thermalized at column densities greater than $\sim 10^{24.5}$ cm^{-2}. The infrared triplet continues to grow in strength beyond this point. The [Ca II] lines also grow relative to X, Y, Z until they too become optically thick.

TABLE 3

PREDICTED EMISSION-LINE SPECTRUM

Ion	λ(Å)	Intensity
H I	4861	1.00
H I	6563	3.06
H^-	fb	0.62
C II	1335	0.14
C III]	1909	3.39
N III]	1750	0.33
N V	1240	0.52
O IV]	1402	0.63
O VI	1035	1.94
Si III]	1895	0.28
Ca II	3934	0.022
Ca II	8498	0.059
Ca II	8662	0.061
Ca II	7324	0.013
Fe	Kα	0.094
H I	1216	13.45
H I	BaC	4.31
C II]	2326	0.14
C III	977	0.60
C IV	1549	11.27
N IV]	1486	0.60
O III]	1663	1.86
O V	1218	0.85
Al III	1860	0.02
Si IV	1397	0.61
Ca II	3969	0.019
Ca II	8542	0.066
Ca II	7291	0.016
Fe II	Total	4.07

Eventually, the C^0 ionization front is reached, and lines of [C I] and [O I] increase in strength. The strongest line formed at great depth is predicted to be [C I] λ8727; atomic data for this line are taken from Pequignot and Aldrovandi (1976) and Mendoza (1983). The more familiar [O I] $\lambda\lambda$6300, 6363 lines also grow strong at very large column densities. All of these forbidden lines saturate when their optical depths eventually exceed unity. The upper limit to the [C I] line, general upper limits to the strength of broad [O I] lines, together with the observed X, Y, Z/Hα and F1, F2/X, Y, Z ratios, together impose no limit to the column density of this cloud.

Conventional wisdom has been that BLR clouds have column densities very close to 10^{23} cm^{-2} (Kwan and Krolik 1981). This was largely based on the claim that the C II] λ2336 line increased with increasing column density. This is not the case for the present calculations. The optical depth in this intercombination line reaches nearly 10^4 for the thicker models; line thermalization, together with the fact that the Balmer continuum optical depth can be large, prevents the C II] line from becoming very strong. Apparently neither line optical depth nor Balmer continuum absorption were taken into account by Kwan and Krolik (see also Collin-Souffrin *et al.* 1986).

V. DISCUSSION

The previous sections have summarized observations of the Ca II spectra of active galaxies and have presented photoionization calculations to examine their consequences. Models with "standard" parameters do not reproduce the observed calcium spectrum; the biggest problem is that the infrared triplet is predicted to be well over an order of magnitude weaker than observed, relative to the hydrogen or other lines. The observation of strong triplet emission, as well as a small K, H/X, Y, Z ratio, leads directly to consideration of clouds with much larger than "standard" column densities. We have included several processes which result in heating at great depth in the clouds, mainly H^0 free-free, excited state photoionization, H^- bound-free, and Compton recoil ionization. These processes result in Ca II infrared triplet and hydrogen Balmer emission which is strong relative to the K, H or Lyα lines. The hydrogen, carbon (including C III] λ1909), and calcium spectrum can be reproduced with an ionization parameter and density deduced from reverberation studies, such as those summarized by Peterson (1988). Large column densities and large ionization parameters solve several problems with current models.

The main results of this paper are the result of a direct confrontation between observations and model calculations, and are as follows:

1. The observed and predicted C III] λ1909/C IV λ1549 intensity ratio suggests that the density is not much above 10^{10} cm^{-3}, as was stressed by Davidson and Netzer (1979). However, the calculations show that a wide range of ionization parameters is allowed, as long as the ionization parameter is large ($U > 10^{-2}$). High ionization parameters deduced by some reverberation studies *are* fully consistent with photoionization model calculations. A result of large ionization parameters is that the intensities of high ionization lines such as O VI 1034 can be reproduced in a one-component model. Another result is that cloud pressure is dominated by radiation pressure. Such a cloud cannot be supported by an external medium (Ferland and Elitzur 1984).

2. The Ca II spectrum is a powerful probe of neutral regions of the BLR, even more so than is Fe II. Its interpretation is straightforward because only five levels are involved, and the atomic data are well determined. We find that no value of N or U can reproduce the Ca II spectrum, given the observed continuum, unless a large column density is assumed. In particular, the predicted intensity of the infrared triplet relative to the hydrogen lines misses the observed ratio by well over an order of magnitude, for standard assumptions. The ratio of the forbidden lines relative to the triplet does suggest densities of order canonical BLR values, $\sim 10^9$ cm^{-3}.

3. The Ca II spectrum, as well as the hydrogen and carbon spectra, *can* be reproduced if the column density is greater than $10^{24.5}$ cm^{-2}. In this case, free-free and Compton recoil heating and excited state photoionization deposit large amounts of energy in the clouds at great depths. This energy is liberated mainly as continua and hydrogen lines. This is a lower limit to the column density in these Fe II emitters. The observed emission-line spectrum actually imposes no strong limit on how great the column density might be.

The main result of this paper is that a single-component model can, to first order, reproduce the observed hydrogen, carbon, and calcium emission-line spectrum, using the observed continuum and the ionization parameter suggested by reverberation studies. This only occurs, however, if the cloud column density is large. The fact that the cloud pressure is dominated by radiation pressure, and that there is no observational limit to the column density, suggests a picture of BLR clouds far different from the conventional one. A cloud supported by radiation pressure will be unstable unless it is self-gravitating. This opens the possibility that BLR clouds are actually winds or coronae surrounding stars (Edwards 1980; Penston 1988) or above an accretion disk. This may also account for a puzzling result found by Rees, Netzer, and Ferland (1989); they found that observations do not require that the BLR stop at some inner radius (the emissivity from clouds very close to the central object is very small), but that the BLR does have a sharp outer boundary. Unobserved [O III] lines, especially λ4363, are produced if the BLR extends beyond a certain outer radius. If the BLR is indeed a wind created by radiation pressure, then the BLR is in fact expected to cease abruptly, when the radiation pressure falls below the confinement pressure for the underlying star or disk. In this situation, BLR clouds would exist only in the "forbidden" region found by Elitzur and Ferland (1986). Radiation driving of a wind is, of course, much more efficient than previously thought, given the higher radiation densities deduced by recent reverberation studies.

We have not been concerned here with line profiles, but rather with the global emission-line spectrum, and the question of whether it can be reproduced, to first order, by a single cloud. The results are surprisingly successful. Line profile studies (Gaskell 1982) show that the BLR is stratified to some extent, however. The next step is to follow the consequences of the calculations presented in this paper to their logical conclusion. Cloud pressure is dominated by radiation pressure, so it seems likely that the BLR is some type of flow. The wind described above may be the site where the observed line shifts and asymmetries occur.

We thank the NSF for support, most recently through grants AST 84-01798 and AST 87-19607. Many comparisons and discussions with H. Netzer were essential. Informative

conversations with E. R. Avrett, J. A. Baldwin, G. H. Newsom, and B. M. Peterson are gratefully acknowledged, along with the thoughtful comments of the referee, S. Collin-Souffrin. The fact that Cloudy reproduced the observed C III] λ1909 to C IV λ1549 ratio at high ionization parameters was first pointed out to G. J. F. by R. J. Weymann at the 1984 Santa Cruz AGN Conference.

APPENDIX

CALCIUM AND CARBON LINE RATIOS AND UPPER LIMITS

I. Ca K-LINE DATA

The K line is seen with some certainty in I Zw 1, where the line strength is consistent with the upper limits for the other objects. It is possible that the K line was also detected in Mrk 493, as a bump appears in Osterbrock and Pogge's (1985) spectrum. It is not at precisely the correct wavelength, however, and its identification as Ca K is doubtful. For the rest of the objects, the Ca K line fluxes or 3 σ upper limits were found from equivalent widths on published spectra, combined with the spectral energy distributions of de Bruyn and Sargent (1978). Table 4 lists the Ca II emitters from Table 4 of P88. Column (2) contains the upper limits to the line fluxes in units of ergs cm^{-2} s^{-1}, and column (4) lists the ratio with respect to XYZ, the sum of the strengths of the triplet lines. The ratio upper limits have been corrected for reddening according to $E_{B-V} = 0.25$ as noted in Table 4; this amounts to a factor of 2.

Two effects cause the K line upper limits to be somewhat uncertain. First, placement of the continuum is difficult in the crowded spectral region around 3934 Å. Second, the underlying galaxy could have the calcium lines in absorption. In several cases noted in P88, stellar calcium triplet lines were found to cause narrow reversals of the emission-line profiles. Present data are not of sufficient accuracy or resolution to allow us to make strong statements about such effects (or the lack thereof) in the region of the K line. We conclude that the best quality K line upper limits (and one measured value) are consistent with KH/XYZ being at least 3 times smaller than the "standard" model predicts.

II. FORBIDDEN CALCIUM LINE DATA

There are little published observational data in the region of F1 and F2; until now the forbidden lines have been definitely detected only in I Zw 1 (Phillips 1976). We have obtained new spectra of a number of AGNs in order to measure accurate line profiles (Morris *et al.* 1989). These data cover the wavelength region of interest at a spectral dispersion of 3 Å per pixel, giving a FWHM resolution element of 7 Å. The spectra of eight AGNs that have the calcium triplet lines in emission were studied, with the result that in no case was any evidence found for [Ca II] line emission. Column (5) of Table 4 lists the 3 σ upper limits.

The redshifts of several of the objects put the forbidden lies close to or within the atmospheric A band, which appears 1.5 mag deep at this spectral resolution. Different data reduction procedures were tried in order to maximize the detectability of the lines even within the A band. Another problem is that the [O II] doublet at 7319, 7330 Å can confuse the detection of F2 at λ7324. For example, in the case of Mrk 42 there is a 4 σ bump at the position of F2, but nothing at F1. This galaxy has strong [S II] emission which also accompanies [O II] emission in Mrk 766. Table 4 lists 3 σ upper limits determined from the noise in the region of the lines, and the upper limits to the [Ca II]/Ca II line ratio F1 + F2/XYZ. On average, the 3 σ upper limit for a detection of either F1 or F2 is $\sim 5\%$ of the local continuum in roughly two resolution elements, depending on the source of the noise in the vicinity of the two lines. Column (5) lists the 3 σ upper limit to log (F1 or F2) in ergs cm^{-2} s^{-1}, using published continuum flux densities (de Bruyn and

TABLE 4

CALCIUM AND CARBON LINE DATA

AGN (1)	Ca K (2)	KH/XYZ[a] (3)	KH/XYZ[b] (4)	Reference (5)	F1 (6)	F/XYZ[c] (7)	Notes (8)	[C I] (9)	[C I]/XYZ (10)
I Zw 1	−13.92	0.14	<0.08	1, 2	−14.05	0.09	1	< −14.39	<0.01
Mrk 42	< −14.83	<0.19	<0.10	3, 4	< −15.11	<0.06	2	< −14.81	<0.05
Mrk 478	< −14.55	<0.10	<0.05	2	< −14.13	<0.14	3	< −14.29	<0.05
II Zw 136	< −13.84	<0.51	<0.31	2	< −14.08	<0.16	3	< −14.53	<0.03
Mrk 231	< −14.01	<0.17	<0.17	5	< −13.97	<0.04	4	< −14.09	<0.01
3C 273	< −13.38	<0.38	<0.20	6, 7	...	...		< −13.69	<0.05
Mrk 486	< −13.97	<1.38	<0.63	8	< −14.70	<0.12	5	< −14.76	<0.05
Mrk 1239	< −13.37	<0.76	<0.43	9	...	...		< −13.82	<0.07
Mrk 766	...	...	...		< −14.33	<0.16	2	< −14.13	<0.13
Zw 033+45	< −14.34	<0.18	<0.12	10	...	...		< −14.21	<0.06
Mrk 684	...	...	...		< −14.52	<0.18	6	< −14.56	<0.08
Mrk 335	< −13.59	<2.80	<1.59	2	...	...		...	...
Mrk 376	< −14.14	<0.67	<0.46	2	...	...		< −14.04	<0.22
Mrk 493	< −14.65	<0.63	<0.33	3	< −15.00	<0.15		< −14.97	<0.08

[a] KH/XYZ line ratios, assuming that every AGN is reddened by $E_{B-V} = 0.25$, in accordance with the results of De Zotti and Gaskell 1985.

[b] KH/XYZ line ratios, including corrections for galactic reddening only.

[c] F indicates the sum of the intensities of F1 and F2.

REFERENCES.—(1) Phillips 1976. (2) Phillips 1977. (3) Osterbrock and Pogge 1985. (4) Koski 1978. (5) Boksenberg *et al.* 1978. (6) Baldwin 1975. (7) Morris and Ward 1988. (8) Schmidt and Miller 1985. (9) Rafanelli and Bonoli 1984. (10) Kunth and Sargent 1979.

NOTES.—(1) Data of Phillips 1976 were used. (2) [O II] doublet is detected, but F1 is not. (3) Mrk 478 and II Zw 136 present special (and uncertain) cases; see text. (4) The A band is a problem for both F1 and F2. (5) the A band is a serious problem for F2. (6) The A band is a serious problem for F1.

Sargent 1978 or Table 4 of P88). Converting to the measured line widths of the triplet lines (Table 3 in P88) and doubling the limits to account for both forbidden lines leads to the ratio upper limits in column (6). The small corrections for reddening between 7324 and 8500 Å were ignored.

Two cases deserve further explanation. There is a clear bump in the spectrum of Mrk 478 at the position of the [Ca II] lines, but it is only half as wide as other BLR lines, including those of the triplet. We have taken the measured equivalent width of the bump as a 3 σ upper limit to the strength of [Ca II]. In column (6) for II Zw 136 there is an emission feature at $7324(1 + z)$ but nothing at $7291(1 + z)$. It is too wide to be due solely to [O II] on the basis of the [S II] line widths. We take the measured equivalent width as a 3 σ upper limit to [Ca II].

III. FORBIDDEN CARBON LINE DATA

The spectra presented in P88 were searched for [C I] λ8727 emission; in no case was the line seen. Table 4 contains the 3 σ upper limits and ratios; the units and ratios are analogous to those of the [Ca II] lines.

APPENDIX B

NUMERICAL DETAILS

This section describes the changes made to the radiative equilibrium code CLOUDY to treat very thick clouds. This discussion refers to version 73 of the code.

I. THE H^- BALANCE: RADIATIVE PROCESSES

Although only a trace amount of hydrogen is in the form of H^-, the opacity provided by this ion is large and helps couple the infrared continuum luminosity to BLR gas. The methods and approximations we employ to include heating and cooling by H^- are described here. Other discussions can be found in Lambert and Pagel (1968), Vernazza, Avrett, and Loeser (1981), and Lites and Mihalas (1984).

We solve for the equilibrium density of H^- by assuming statistical equilibrium and balancing production and destruction mechanisms. We take great care in including both forward and back reactions to ensure that the present treatment of H^- is capable to going to LTE in the limit of high radiation or particle densities.

In much of the following discussion, we will compare the predicted H^- population with its LTE value. The LTE relative population density of H^- is

$$P^*(H^-) = \frac{N^*_{H^-}}{N_e N_{H^0}} = \frac{g_{H^-}}{g_H g_e}\left(\frac{h^2}{2\pi mkT}\right)^{3/2} \exp\left(\chi_{H^-}/kT\right) \text{ cm}^3 , \tag{B1}$$

where g_i is the statistical weight of the constituents, $\chi_{H^-} = 0.055502$ Ry is the binding energy of the negative hydrogen ion, and other constants have their usual meaning. The reaction network also includes H_2, H_2^+, and HeH^+; this will be the subject of a future paper. The LTE relative population densities of H_2, H_2^+, and HeH^+ are defined similarly and are denoted by $P^*(H_2)$, $P^*(H_2^+)$, and $P^*(HeH^+)$.

a) Radiative Attachment

Radiative attachment is the most important creation mechanism for H^- at low densities, when three-body processes are negligible:

$$H^0 + e^- \Rightarrow H^- + \gamma . \tag{B2}$$

The rate coefficient is evaluated by numerically integrating the photodetachment cross section over frequency:

$$\alpha_{rad}(T) = P^*(H^-)\int_{\nu_0}^{\infty} \sigma_{bf}\frac{8\pi\nu^2}{c^2}\exp\left(-h\nu/kT\right)d\nu \text{ cm}^3 \text{ s}^{-1} , \tag{B3}$$

where we use cross sections computed by Wishart (1979) and spline interpolation. These cross sections are in excellent agreement with the velocity operator bound-free cross sections tabulated by Doughty, Fraser, and McEachran (1966). The energy interval between the photodetachment threshold at 0.055502 and $\sim$1.8 Ry is divided into roughly 100 cells with logarithmically increasing width, and the integration is carried out as a straightforward sum.

Tests show that the numerical radiative attachment rates computed here are in very good agreement with the approximation given by Hutchins (1976), who used the cross sections computed by Doughty, Fraser, and McEachran (1966), for temperatures 500 K $\leq T \leq$ 2500 K (notice that there is a typographical error in the approximation for the radiative attachment rate given by Palla, Salpeter, and Stahler 1983). It is also within 10% of the value given by Dalgarno and Kingston (1963), which was based on earlier calculations of the photodetachment cross section.

Continuum occupation numbers can be large in the infrared. The induced radiative attachment rate coefficient is

$$\alpha_{ind}(T) = P^*(H^-)\int_{\nu_0}^{\infty} \sigma_{bf}\frac{4\pi J_\nu(\tau)}{h\nu}\exp\left(-h\nu/kT\right)d\nu \text{ cm}^3 \text{ s}^{-1} , \tag{B4}$$

where the mean intensity of the depth-dependent continuum is $J_\nu(\tau)$.

b) Photodetachment

Photodetachment

$$H^- + \gamma \Rightarrow H^0 + e^- , \tag{B5}$$

is the dominant H^- destruction mechanism for typical BLR conditions. The rate is evaluated in the standard manner:

$$\Gamma(H^-) = \int_{\nu_0}^{\infty} \sigma_{bf} \frac{4\pi J_\nu(\tau)}{h\nu} d\nu \ s^{-1} . \tag{B6}$$

The integral is evaluated as a sum over the numerically binned continuum. The incident continuum is then attenuated by optical depth increments

$$d\tau = \sigma_{bf} N_{H^-}[1 - \exp(-h\nu/kT)/b_{H^-}]dr , \tag{B7}$$

where b_{H^-} is the departure coefficient for H^-, $b_{H^-} \equiv N(H^-)/N^*(H^-)$, where $N^*(H^-)$ is the LTE H^- density.

c) Photodetachment by Hard Photons

The H^- photoabsorption cross section increases above $\sim\frac{3}{4}$ Ry, energies where excitation of $n \geq 2$ levels is possible. Cross sections which include this process are taken from Broad and Reinhardt (1976). These calculations do no extend to high energies, so we scale high-energy hydrogen cross sections by the ratio of H^- to H^0 cross sections at 18 Å in order to take absorption of X- and γ-rays into account.

The cross section for $(\gamma, 2e^-)$ absorption is much smaller than (γ, e^-) (Broad and Reinhardt 1976), and this latter process is neglected.

d) The Approach to LTE: High-Radiation Densities

As a test of our assumptions and methods, we consider the approach to LTE under conditions dominated by radiative attachment (spontaneous and induced) and photodetachment. Tests in which gas with temperature T_e is exposed to blackbody radiation fields with color temperature T_B were computed. The color and gas temperatures were set equal, $T_e = T_B$, and the intensity of the radiation field was varied up to the blackbody limit. The intensity of the radiation field is parameterized by the equivalent energy density temperature $T_U = (U/a)^{1/4}$, where U is the energy density (see Ferland and Rees 1988) and a is the Stefan's radiation density constant. The equilibrium population of H^- was computed, including all processes mentioned below, but with the hydrogen density small enough (typically $\sim 10^5$ cm^{-3}) for radiative processes to be most important. The H^- population is expressed as a departure coefficient, and the results are shown in the upper panel of Figure 9, for tests in which $T_B = 0.5$, 1, and 2×10^4 K. When $T_u = T_B$, and the radiation field is in strict thermodynamic equilibrium radiative processes must hold H^- in LTE, and departure coefficients of unity are expected. The computed departure coefficients for the three temperatures are 0.9998, 0.9996, and 1.0030, respectively. As the figure shows, when T_u is lowered below T_B, the intensity of the radiation field falls below its thermodynamic equilibrium value and the population of H^- increases. This is because the photodetachment rate (which is proportional to the intensity of the radiation field) is no longer in balance with the radiative attachment rate (which is proportional only to the electron density).

II. THE H^- BALANCE: COLLISIONAL PROCESSES

a) Associative Detachment

The most important H_2 formation mechanism in dust-free environments, and a significant H^- destruction mechanism, is associative detachment

$$H^- + H^0 \rightleftharpoons H_2 + e^- , \tag{B8}$$

where we use rate coefficients from Bieniek and Dalgarno (1979). The reverse reaction rate coefficient C_R, for electron collisional dissociation of H_2, is related to the forward rate coefficient C_F by detailed balance:

$$C_R = C_F \frac{P^*(H^-)}{P^*(H_2)} . \tag{B9}$$

b) Electron Collisional Detachment

For typical BLR temperatures and ionization fractions, the process

$$H^- + e^- \rightleftharpoons H + 2e^- \tag{B10}$$

is a competitive H^- destruction mechanism. We use rates taken from the compendium of Janev *et al.* (1987). The reverse process, electron three-body recombination with neutral hydrogen, is included via detailed balance

$$C_R = C_F P^*(H^-) . \tag{B11}$$

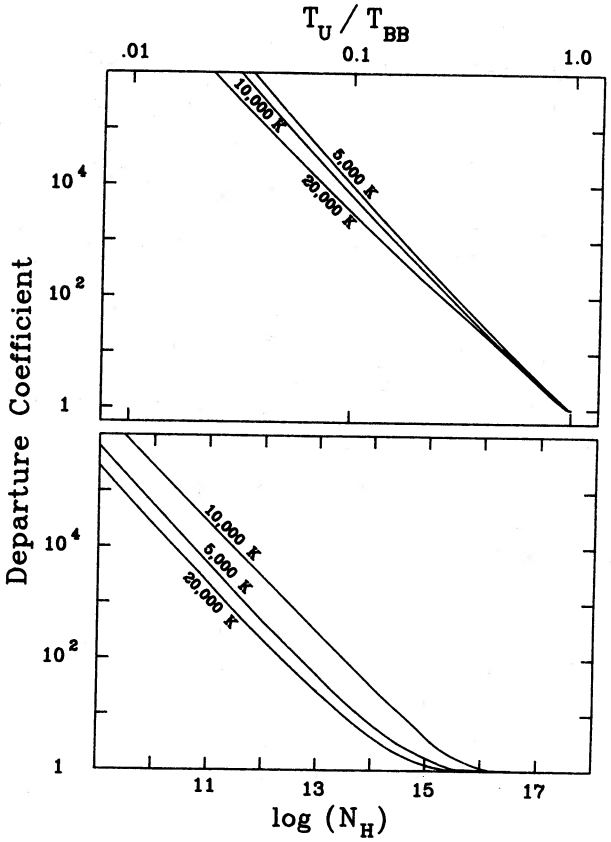

FIG. 9.—H-departure coefficients. Upper panel shows the results of a series of calculations in which hydrogen density was held fixed at relatively low densities (typically $N_H \sim 10^5$ cm^{-3}), and the gas irradiation with blackbody radiation fields with color temperatures of 5, 10, and 20 × 10^3 K. Gas temperature was set to the color temperature. Intensity of the radiation field was varied up to its LTE limit and is characterized as an equivalent energy density temperature T_U. This test case shows that the model hydrogen atom goes to LTE (departure coefficients of unity) when spontaneous and induced processes occur in the appropriate balance. Lower panel shows a similar test in which the radiation density was low but the hydrogen density varied over a wide range. Three gas temperatures, spanning the range encountered in typical BLR calculations, are shown. Collisional processes, both two- and three-body, bring the gas to LTE at high densities.

c) Collisional Ionization by Suprathermal Electrons

The total suprathermal collisional ionization rate is computed using approximation from Shull and Van Steenberg (1985). Ionization of H^- by suprathermal electrons is scaled from the H^0 rates using cross sections at 20 eV given by Janev *et al.* (1987). This energy was chosen as representative of the mean energy of the secondary electron shower. The majority of these collisions are of the form $e^- + H^- \Rightarrow H(1s) + 2e^-$, although $e^- + H^- \Rightarrow H^+ + 3e^-$ collisions occur roughly 1% of the time.

d) Mutual Neutralization

Ionized hydrogen can charge transfer with the negative ion through

$$H^- + H^+ \rightleftharpoons H + H^* . \tag{B12}$$

We use the rate coefficients given in Janev *et al.* (1987). By far the largest rate coefficients are for collisions which populate hydrogen in the $n = 3$ level. These rates are based on both experimental and theoretical data (see, for example, Peart, Bennett, and Dolder 1985).

The reverse reaction is included using detailed balance; if the rate coefficient for the forward reaction is C_F, then the reverse reaction rate, and its rate coefficient C_R, are given by

$$H(1s)N(i)C_R = b_i P^*(H^-)N_e N_p C_F , \tag{B13}$$

where $N(i)$ and b_i are the population and departure coefficient of hydrogen in the ith level.

e) Charge Neutralization with Heavy Elements

The process

$$H^- + A^+ \rightleftharpoons H^0 + A^0 \tag{B14}$$

is considered by Dalgarno and McCray (1973), who give rate coefficients for very low temperatures and ionization levels. Judging from the curves given by Peterson *et al.* (1971), upon which the Dalgarno and McCray rates are based, the approximation they give

should still be valid (although very uncertain) at temperatures of interest here (~ 0.5–1.0×10^4 K). Here A^+ is all singly ionized species, which are assumed to be neutralized at the same rate.

f) Neglected Processes

Of the possible destruction mechanisms, we neglect collisional detachment by protons ($p^+ + H^- \Rightarrow H + p^+ + e^-$), which has a negligible rate coefficient according to Janev *et al.* (1987), and collisional detachment by atomic hydrogen ($H^- + H \Rightarrow 2H + e^-$), which has no reliable rate coefficient according to Lites and Mihalas (1984).

g) The Approach to LTE: High-Hydrogen Densities

A series of models in collisional equilibrium were computed. Radiative processes were also included, but the incident radiation field, a 10^4 K blackbody, was given a negligible intensity (an ionization parameter of $U = 10^{-12}$). Three temperatures, 0.5, 1, and 2×10^4 K, were considered to span the temperature range of interest in the following BLR calculations. The hydrogen density was varied between 10^8 and 10^{18} cm^{-3} to confirm the approach to LTE at high densities. The results of these calculations are shown in the lower panel of Figure 9. For the majority of the calculations hydrogen is largely neutral, and for the smaller temperatures a significant fraction of the hydrogen was in the molecular form (H_2 and H_2^+). The calculation confirms that the departure coefficients were within 2% of unity at the highest densities computed.

III. H^- HEATING AND COOLING

The calculation of the heating and cooling rates due to H^- are described here. As is customary in the interstellar medium literature, we define heating and cooling relative to the continuum, so that ionization of an atom or ion with ionization potential $h\nu_0$ by a photon with energy $h\nu$ produces $h(\nu - \nu_0)$ of heat.

a) H^- Bound-Free

The volume heating rate due to spontaneous absorption (photodetachment) is

$$G_{H^-} = N(H^-) \int_{\nu_0}^{\infty} \frac{4\pi J_\nu}{h\nu} \sigma_{bf} h(\nu - \nu_0) d\nu \text{ ergs s}^{-1} \text{ cm}^{-3} , \tag{B15}$$

where symbols have their usual meaning. The volume cooling rate due to induced radiative attachment is

$$\Lambda_{ind,H^-} = N_e N_{H^0} P^*(H^-) \int_{\nu_0}^{\infty} \sigma_{bf} \frac{4\pi J_\nu}{h\nu} \exp(-h\nu/kT) h(\nu - \nu_0) d\nu \text{ ergs s}^{-1} \text{ cm}^{-3} , \tag{B16}$$

while the volume cooling rate for spontaneous radiative attachment is

$$\Lambda_{spon,H^-} = N_e N_{H^0} 8\pi P^*(H^-) \int_{\nu_0}^{\infty} \sigma_{bf} \frac{\nu^2}{c^2} \exp(-h\nu/kT) h(\nu - \nu_0) d\nu . \tag{B17}$$

b) H^- Free-Free

Free-free heating and cooling by H^- is also significant, although less so than bound-free heating. This is included, making the appropriate correction for stimulated emission, using the cross sections given by Vernazza, Avrett, and Loeser (1981; see also Bell, Kingston, and McIlveen 1975). In the following calculations, H^- bound-free heating and cooling is much more important than free-free processes. This is surprising at first sight, since standard opacity curves comparing bound-free and free-free opacities (Bell, Kingston, and McIlveen 1975; Mihalas 1978) show that the two are comparable. These curves are for LTE, with departure coefficients of unity. The departure coefficient for H^- is actually many orders of magnitude larger than unity in the following calculations, so that the bound-free opacity and the resulting heating greatly exceeds the free-free opacity.

IV. MOLECULAR HYDROGEN

CLOUDY has included the ion-molecule scheme described by Black (1978) and Hollenbach and McKee (1979) for the past 10 yr. A brief account was given by Ferland (1980). Recently, Kallman, Lepp, and Giovannoni (1987; hereafter KLG) computed the molecular hydrogen density for typical conditions in BLR clouds. They found conditions in which a substantial fraction of the hydrogen was molecular. In the present calculations, H_2 is a trace species at best.

For dust-free environments, H_2 forms mainly through associative detachment from H^-, and the H_2 population is linearly coupled to the H^- fraction. The latter must be calculated with great precision. Apparently, the only H^- destruction mechanism considered by KLG is associative detachment to form H_2. Actually many processes, especially photodetachment but collisions as well, compete with H_2 in the destruction of H^-. As a result, only a small fraction of H^- creations eventually result in the formation of H_2 in our calculations, and the predicted H_2 abundance is small.

REFERENCES

Aldrovandi, S. M. V., and Pequignot, D. 1974, *Rev. Brasiliera Fis.*, **4**, 491.
Arnaud, M., and Rothenflug, R. 1985, *Astr. Ap. Suppl.*, **60**, 425.
Avrett, E. H., and Loeser, R. 1988, *Ap. J.*, **331**, 211.
Baldwin, J. A. 1975, *Ap. J.*, **201**, 26.
———. 1977, *M.N.R.A.S.*, **178**, 67.
Baldwin, J. A., and Netzer, H. 1978, *Ap. J.*, **226**, 1.
Baldwin, J. A., Wampler, E. J., and Gaskell, C. M. 1988, *Ap. J.*, **338**, 630.
Bell, K. L., Kingston, A. E., and McIlveen, W. A. 1975, *J. Phys. B*, **8**, 358.
Bethe, H. A., and Salpeter, E. E. 1957, *The Quantum Mechanics of One- and Two-Electron Atoms* (New York: Academic).
Bieniek, R. J., and Dalgarno, A. 1979, *Ap. J.*, **228**, 635.
Black, J. H. 1978, *Ap. J.*, **222**, 125.

Black, J. H., Weisheit, J. C., and Laviana, E. 1972, *Ap. J.*, **177**, 567.
Boksenberg, A., Carswell, R. F., Allen, D. A., Fosbury, R. A. E., Penston, M. V., and Sargent, W. L. W. 1977, *M.N.R.A.S.*, **178**, 451.
Broad, J. T., and Reinhardt, W. P. 1976, *Phys. Rev.*, *A*, **14**, 2159.
Butler, S. E., and Dalgarno, A. 1980, *Ap. J.*, **838**, 107.
Cameron, A. G. W. 1982, in *Essays in Nuclear Astrophysics*, ed. C. Barnes, D. Clayton, and D. Schramm (London: Cambridge University Press), p. 34.
Chidichimo, M. C. 1981, *J. Phys. B*, **14**, 4149.
Collin-Souffrin, S. 1986, *Astr. Ap.*, **166**, 115.
———. 1987, *Astr. Ap.*, **179**, 60.
Collin-Souffrin, S., Dumont, S., Joly, M., and Pequignot, D. 1986, *Astr. Ap.*, **166**, 27.
Collin-Souffrin, S., Hameury, J. M., and Joly, M. 1988, preprint.
Collin-Souffrin, S., and Lasota, J. 1988, *Pub. A.S.P.*, **100**, 1041.
Dahari, O., and De Robertis, M. M. 1988, *Ap. J. Suppl.*, **67**, 249.
Dalgarno, A., and Kingston, A. E. 1963, *Observatory*, **83**, 39.
Dalgarno, A., and McCray, R. A., 1973, *Ap. J.*, **181**, 95.
Davidson, K. 1977, *Ap. J.*, **218**, 20.
Davidson, K., and Netzer, H. 1979, *Rev. Mod. Phys.*, **51**, 715.
de Bruyn, A. G., and Sargent, W. L. W. 1978, *A.J.*, **83**, 1257.
De Zotti, G., and Gaskell, C. M. 1985, *Astr. Ap.*, **147**, 1.
Doughty, N. A., Fraser, P. A., and McEachran, R. P. 1966, *M.N.R.A.S.*, **132**, 255.
Edwards, A. C. 1980, *M.N.R.A.S.*, **190**, 757.
Elitzur, M., and Ferland, G. J. 1986, *Ap. J.*, **305**, 35.
Elitzur, M., and Netzer, H. 1985, *Ap. J.*, **291**, 464.
Engargiola, G., Harper, D. A., Elvis, M., and Willner, S. P. 1988, *Ap. J. (Letters)*, **332**, L19.
Ferland, G. J., 1980, *Bull. AAS*, **12**, 853.
———. 1988, OSU Int. Rep. No. 88–001.
Ferland, G. J., and Elitzur, M. 1984, *Ap. J. (Letters)*, **285**, L11.
Ferland, G. J., and Netzer, H. 1979, *Ap. J.*, **229**, 274.
Ferland, G. J., and Rees, M. J. 1988, *Ap. J.*, **332**, 141.
Gaskell, C. M. 1982, *Ap. J.*, **263**, 79.
Grandi, S. A. 1983, *Ap. J.*, **268**, 591.
Grandi, S. A., and Osterbrock, D. E. 1977, *Ap. J.*, **220**, 783.
Halpern, J. P., and Oke, J. B. 1987, *Ap. J.*, **312**, 91.
Hamilton, D., and Keel, W. C. 1987, *Ap. J.*, **321**, 211.
Herbig, G. H., and Soderblom, D. R. 1980, *Ap. J.*, **242**, 628.
Hollenbach, D., and McKee, C. F. 1979, *Ap. J. Suppl.*, **41**, 555.
Hubbard, E. M., and Puetter, R. C. 1985, *Ap. J.*, **290**, 394.
Hummer, D. G. 1988, *Ap. J.*, **327**, 477.
Hutchins, J. B. 1976, *Ap. J.*, **205**, 103.
Janev, R. K., Langer, W. D., Post, D. E., and Evans, K. 1987, *Elementary Processes in Hydrogen—Helium Plasmas* (Berlin: Springer).
Joly, M. 1986, in *IAU Symposium 119*, *Quasars*, ed. G. Swarup and V. K. Kapahi (Dordrecht: Reidel), p. 337.
———. 1988, *Astr. Ap.*, **208**, 47.
Jordan, C. 1969, *M.N.R.A.S.*, **142**, 501.
Kallman, T., Lepp, S., and Giovannoni, P. 1987, *Ap. J.*, **321**, 907.
Koski, A. T. 1978, *Ap. J.*, **223**, 56.
Kriss, G. A., Canizares, C. R., and Ricker, G. R. 1980, *Ap. J.*, **242**, 492.
Krolik, J., McKee, C., and Tarter, C. B. 1981, *Ap. J.*, **249**, 422.
Kunth, D., and Sargent, W. L. W. 1979, *Astr. Ap.*, **76**, 50.
Kwan, J., and Krolik, J. 1981, *Ap. J.*, **250**, 478.
Lambert, D. L., and Pagel, B. E. J. 1968, *M.N.R.A.S.*, **141**, 299.
Lites, B. W., and Mihalas, D. 1984, *Solar Phys.*, **93**, 23.
Malkan, M. A., and Sargent, W. L. W. 1982, *Ap. J.*, **254**, 122.
Mathews, W. G., and Ferland, G. J. 1987, *Ap. J.*, **323**, 456.
Mendoza, C. 1983, in *IAU Symposium 103*, *Planetary Nebulae*, ed. D. R. Flower (Dordrecht: Reidel), p. 143.
Mihalas, D. 1978, *Stellar Astropheres* (2d ed.; San Francisco: Freeman).
Morris, S. L., Boroson, T., Persson, S. E., and Meyers, K. 1989, in preparation.
Netzer, H. 1985, *Ap. J.*, **289**, 451.
Netzer, H. 1989, *Proc. Santa Cruz Conf.*, in press.
Netzer, H., Elitzur, M., and Ferland, G. J. 1985, *Ap. J.*, **299**, 752.
Netzer, H., and Wills, B. J. 1983, *Ap. J.*, **275**, 445.
Osterbrock, D. E. 1951, *Ap. J.*, **114**, 469.
———. 1974, *Astrophysics of Gaseous Nebulae* (San Francisco: Freeman).
Osterbrock, D. E., and Pogge, R. W. 1985, *Ap. J.*, **297**, 166.
Palla, F., Salpeter, E. E., and Stahler, S. W. 1983, *Ap. J.*, **271**, 632.
Peart, B., Bennett, M. A., and Dolder, K. J. 1985, *J. Phys. B*, **18**, L439.
Penston, M. V. 1988, *M.N.R.A.S.*, **233**, 601.
Pequignot, D., and Aldrovandi, S. 1976, *Astr. Ap.*, **50**, 141.
Persson, S. E. 1988, *Ap. J.*, **330**, 751.
Persson, S. E., and McGregor, P. J. 1985, *Ap. J.*, **290**, 125.
———. 1988, *Pub. A.S.P.*, **100**, 18.
Peterson, B. M., and Gaskell, C. M. 1989, in preparation.
Peterson, J. R., Aberth, W., Moseley, J., and Sheridan, J. 1971, *Phys. Rev. A.*, **3**, 1651.
Phillips, M. M. 1976, *Ap. J.*, **208**, 37.
———. 1977, *Ap. J.*, **215**, 746.
Rafanelli, P., and Bonoli, C. 1984, *Astr. Ap.*, **131**, 186.
Rees, M. J. 1987, *M.N.R.A.S.*, **228**, 47.
Rees, M. J., Netzer, H., and Ferland, G. J. 1989, *Ap. J.*, **347**, 640.
Reilman, R. F., and Manson, S. T. 1979, *Ap. J. Suppl.*, **40**, 815.
Saraph, H. E. 1970, *J. Phys. B*, **3**, 952.
Schmidt, G. D., and Miller, J. S. 1985, *Ap. J.*, **290**, 517.
Shine, R. A., and Linsky, J. L. 1974, *Solar Phys.*, **39**, 49.
Shuder, J. M., and MacAlpine, G. M. 1979, *Ap. J.*, **230**, 348.
Shull, J. M., and Van Steenberg, M. 1982, *Ap. J. Suppl.*, **48**, 95.
———. 1985, *Ap. J.*, **298**, 268.
Vernazza, J. E., Avrett, E. H., and Loeser, C. B. 1981, *Ap. J. Suppl.*, **45**, 635.
Wills, B. J., Netzer, H., and Wills, D. 1985, *Ap. J.*, **288**, 94.
Wishart, A. W. 1979, *M.N.R.A.S.*, **187**, 59.
Zamorani, G., *et al.* 1981, *Ap. J.*, **245**, 357.

GARY J. FERLAND: Astronomy Department, Ohio State University, Columbus, OH 43210

S. ERIC PERSSON: Observatories of the Carnegie Institution of Washington, 813 Santa Barbara St., Pasadena, CA 91101